PNAS RESEARCH ARTICLE | EARTH, ATMOSPHERIC, AND PLANETARY SCIENCES
ENVIRONMENTAL SCIENCES

Quantifying fire-specific smoke exposure and health impacts

Jeff Wen[a,1], Sam Heft-Neal[b], Patrick Baylis[c], Judson Boomhower[d,e], and Marshall Burke[b,e,f]

Edited by Colleen E. Reid, University of Colorado Boulder, Boulder, CO; received June 12, 2023; accepted September 21, 2023 by Editorial Board Member Akkihebbal R. Ravishankara

Rapidly changing wildfire regimes across the Western United States have driven more frequent and severe wildfires, resulting in wide-ranging societal threats from wildfires and wildfire-generated smoke. However, common measures of fire severity focus on what is burned, disregarding the societal impacts of smoke generated from each fire. We combine satellite-derived fire scars, air parcel trajectories from individual fires, and predicted smoke $PM_{2.5}$ to link source fires to resulting smoke $PM_{2.5}$ and health impacts experienced by populations in the contiguous United States from April 2006 to 2020. We quantify fire-specific accumulated smoke exposure based on the cumulative population exposed to smoke $PM_{2.5}$ over the duration of a fire and estimate excess asthma-related emergency department (ED) visits as a result of this exposure. We find that excess asthma visits attributable to each fire are only moderately correlated with common measures of wildfire severity, including burned area, structures destroyed, and suppression cost. Additionally, while recent California fires contributed nearly half of the country's smoke-related excess asthma ED visits during our study period, the most severe individual fire was the 2007 Bugaboo fire in the Southeast. We estimate that a majority of smoke $PM_{2.5}$ comes from sources outside the local jurisdictions where the smoke is experienced, with 87% coming from fires in other counties and 60% from fires in other states. Our approach could enable broad-scale assessment of whether specific fire characteristics affect smoke toxicity or impact, inform cost-effectiveness assessments for allocation of suppression resources, and help clarify the growing transboundary nature of local air quality.

wildfire | air pollution | climate change | health impacts

Significance

Wildfires have rapidly increased across the United States in recent decades, and smoke from these fires is a growing contributor to air pollution. Our understanding of the fire-specific contributions to this growing pollution source remains incomplete, however, limiting comprehensive measurement of the severity and breadth of a given fire's impact. We develop a method to quantify accumulated population smoke $PM_{2.5}$ exposure and asthma-related health impacts for individual fires across the contiguous United States between 2006 and 2020. Our approach provides a method for quantifying the social cost of individual fires and the increasingly transboundary nature of wildfire smoke and can inform how to allocate fire and air quality management resources to best protect communities from this growing wildfire-related risk.

Wildfire regimes have changed in recent decades due to a combination of climate change and a century of fire suppression (1). This increase has driven a greater frequency of large wildfire events that result in physical infrastructure damage from the fire and health-related damages from the fine particulate matter ($PM_{2.5}$) in smoke (2–4). While total $PM_{2.5}$ has been decreasing in the decades since the Clean Air Act, recent evidence suggests that wildfire smoke $PM_{2.5}$ has begun to reverse this trend, especially in the Western United States (5–7). This reversal is concerning as recent research suggests that $PM_{2.5}$ from wildfire smoke could be more toxic than $PM_{2.5}$ from other sources for some health outcomes (4, 8–10) and that existing air quality regulation is poorly equipped to manage smoke from wildfires (7). Smoke $PM_{2.5}$ concentrations have now been well measured at broad temporal and spatial scales in the United States (6, 11), and increasing concentrations have been linked to an array of negative societal outcomes, including respiratory morbidity (12), premature deaths (13), preterm births (14–16), and lower test performance in school-aged children (17), underscoring the growing social costs of wildfire smoke $PM_{2.5}$ exposure.

Despite growing knowledge of the broad-reaching negative impacts of wildfire smoke exposure, commonly used metrics of wildfire severity currently do not reflect the societal harm from smoke. Instead, severity metrics typically focus on the number of structures burned, lives tragically lost in the fire itself, cost of firefighting, and/or total burned area, with the latter a particularly problematic measure given the agreed-upon need for more low-intensity fire (such as prescribed fire) in order to reduce the likelihood of more extreme fires (18–20).

An inability to link specific fires to their smoke impacts is problematic for at least three reasons. First, the health and societal impacts of smoke from specific fires are plausibly a large proportion of their damage, and the lack of information about the magnitude of these damages hampers efforts to understand whether taxpayer-funded wildfire suppression efforts (21, 22) are being allocated to the most damaging fires. Second, it is increasingly hypothesized that the same amount of smoke from different fires need not have equivalent damages, given that some fires (for example) incinerate chemicals in buildings or burn and aerosolize metals or fungi found in specific soils (23–25). But these hypotheses remain hard to test broadly absent a method to link specific smoke exposures to source fire

Author contributions: J.W. and M.B. designed research; J.W. performed research; J.W., S.H.-N., and M.B. contributed new reagents/analytic tools; J.W., S.H.-N., P.B., J.B., and M.B. analyzed data; and J.W., S.H.-N., P.B., J.B., and M.B. wrote the paper.

The authors declare no competing interest.

This article is a PNAS Direct Submission. C.E.R. is a guest editor invited by the Editorial Board.

[1]To whom correspondence may be addressed. Email: jlwen@stanford.edu.

This article contains supporting information online at https://www.pnas.org/lookup/suppl/doi:10.1073/pnas.2309325120/-/DCSupplemental.

Published December 12, 2023.

characteristics at scale. Third, linking smoke exposures to their source fires is important for understanding the transboundary nature of wildfire smoke and in turn for designing strategies and policies to mitigate smoke exposures. Recent increases in the number of exceptional event applications to flag and omit air quality exceedances due to wildfires (26) suggest that the management of transboundary wildfire air pollution is a growing challenge. Although the Environmental Protection Agency (EPA) requires jurisdictions to develop mitigation plans for recurring exceptional events (27) and regional coalitions have been formed to address these issues, the continued transport of smoke across jurisdiction boundaries (28–30) will make it challenging for state, tribal, or local air quality agencies to reduce local $PM_{2.5}$ concentrations by reducing local emissions.

Here, we combine high-resolution estimates of daily smoke $PM_{2.5}$ (6) with a physical model of fire-specific air parcel trajectories from the Hybrid Single-Particle Lagrangian Integrated Trajectory (HYSPLIT) model to develop a method for linking specific source fires to the smoke $PM_{2.5}$ generated by that fire. Our method uses the inverse distance weighted sum of simulated smoke trajectory points to proportionally attribute the daily smoke $PM_{2.5}$ for each 10-km gridcell-day to specific smoke-producing fires. This allows us to estimate the share of smoke that each fire has plausibly contributed to downwind locations. We then use this method to calculate the accumulated smoke exposure from wildfire smoke $PM_{2.5}$ based on the cumulative concentration of smoke $PM_{2.5}$ that populations experience from each fire, for all identified smoke-producing fires between April 2006 and December 2020 (*Methods*). This approach aggregates the $\mu g/m^3$ of smoke $PM_{2.5}$ experienced by the affected population over the duration of exposure to a specific fire. We build on recent work that estimated the effects of wildfire smoke $PM_{2.5}$ exposure on asthma emergency department (ED) visits (31) and calculate fire-specific health impacts (*Methods*). We use these estimates to rank fires by their health impacts. We then compare the estimated number of excess asthma ED visits to other commonly used wildfire severity and suppression effort metrics such as burned area, suppression cost, and structures burned.

Finally, we use our linked estimates to quantify changing patterns and magnitudes of transboundary smoke $PM_{2.5}$ movement, calculating how the regional sources of smoke exposure have changed between an earlier, less smokey 2006 to 2010 period vs. a later more smokey 2016 to 2020 period. We also combine the fire-smoke linked data with estimates of total $PM_{2.5}$ for 11 Western states (32) to quantify the proportion of total $PM_{2.5}$ from out-of-county source fires—a quantity relevant to discussions of how to manage local air quality.

Results

Our method of linking source fires to smoke exposure is shown in Fig. 1, using a particularly active fire period in California in 2018 as an example. During this period, three large active fires generated smoke that covered much of California, and this smoke was readily apparent in satellite imagery, recorded in analyst-delineated smoke plumes (33), and identified in gridded smoke $PM_{2.5}$ data (6) (Fig. 1 *A*–*C*). We associated daily analyst estimates of smoke-producing fire locations with fire extent polygons and ran forward trajectories of smoke particles emitted at each fire location using the HYSPLIT model (Fig. 1*D* and *Methods*). Trajectories were then used to partition the contribution of each source fire to estimated wildfire smoke $PM_{2.5}$ (Fig. 1*E* and *Methods*), and fire-specific accumulated smoke exposure was calculated as the sum of population exposed to each $\mu g/m^3$ of smoke on each day for the duration of each fire (*SI Appendix*, Fig. S1). In total, our analysis includes over 461,000 total smoke generating sources with around 23,900 fires linked to specific burned area polygons identified by NASA's Moderate-Resolution Imaging Spectroradiometer (MODIS) satellite and around 437,500 additional smoke-producing fires that do not fall into burned area polygons (*Methods*).

Validation of our approach on days in which only one fire was burning shows that our approach captures nearly all of the smoke emitted by a given fire and aligns closely with visible satellite imagery on the same day, though we note that satellite resolution constraints can lead to conservative estimates of contributed smoke $PM_{2.5}$ in some cases (*Methods* and *SI Appendix*, Figs. S2 and S3). On days in which multiple fires are burning and locations experience overlapping smoke from multiple fires, fire-specific attributions are less certain, and we thus compute a fire-specific "attribution certainty score" that calculates the percent of a fire's overall attributed smoke exposure that occurs on days when smoke from other fires is not present (*Methods* and *SI Appendix*, Fig. S4); more isolated fires have attributed smoke exposures that are more certain. When comparing against EPA air pollution monitor readings, our approach captures a majority of wildfire-driven air pollution, does not exceed total ground-measure $PM_{2.5}$ concentrations, and shows close alignment with the amount of smoke $PM_{2.5}$ predicted at example EPA air pollution monitoring stations using ground data (Fig. 2 and *SI Appendix*, Fig. S5).

We use the fire-specific accumulated smoke exposure to quantify the number of excess asthma ED visits associated with each fire and use these quantities to rank fires by their health impact (*Methods*). We show the top 9 most impactful fires in Fig. 3 and the top 20 fires in *SI Appendix*, Table S1. Out of the top 9, 6 of the fires are from the 2020 fire season and 7 of these top fires originated in California. Perhaps surprisingly, the Bugaboo fire, which originated in Georgia in 2007 and is the only top fire that originated on the East Coast, is ranked as the fire that resulted in the highest amount of accumulated smoke exposure and highest number of estimated excess asthma ED visits (1,407 95% CI: 1,295 to 1,518), nearly twice the amount estimated for the next fire. This fire spread dense smoke across highly populated areas of the US Southeast for over a month (*SI Appendix*, Fig. S6). The four other fires in the top 5 most severe fires were all in California. Three of these fires—August Complex, Dolan, and Bobcat, all in 2020—were in late summer, a period during which prevailing winds carried smoke across much of the US West and Midwest for weeks (Fig. 3). The August Complex fire, in 2020, generated smoke for more than 2 mo, which resulted in the second highest number of asthma-related ED visits (853 95% CI: 785 to 921) across much of the contiguous US. The fourth, the 2018 Camp Fire, was during late fall, where easterly winds blew thick smoke into highly populated CA regions for a short period. We calculate that the Camp Fire generated the highest average daily smoke $PM_{2.5}$ concentration across gridcells in our sample, with the Bugaboo Fire second (*SI Appendix*, Table S1). Other fires in the top ten tended to be late summer fires on the West Coast (CA and OR), where large amounts of smoke were again blown east across much of the US West and Midwest. Our ranking of fires by health impact would be preserved for any health outcome beyond asthma [e.g., mortality (36)] where counts or rates of the outcome are thought to have a linear relationship with smoke exposure, although the aggregate health burden could differ by outcome.

We compare the number of excess asthma ED visits for each fire with different commonly used wildfire severity and suppression effort metrics, including burned area, structures burned (37), and fire suppression cost (38). The number of excess asthma ED visits

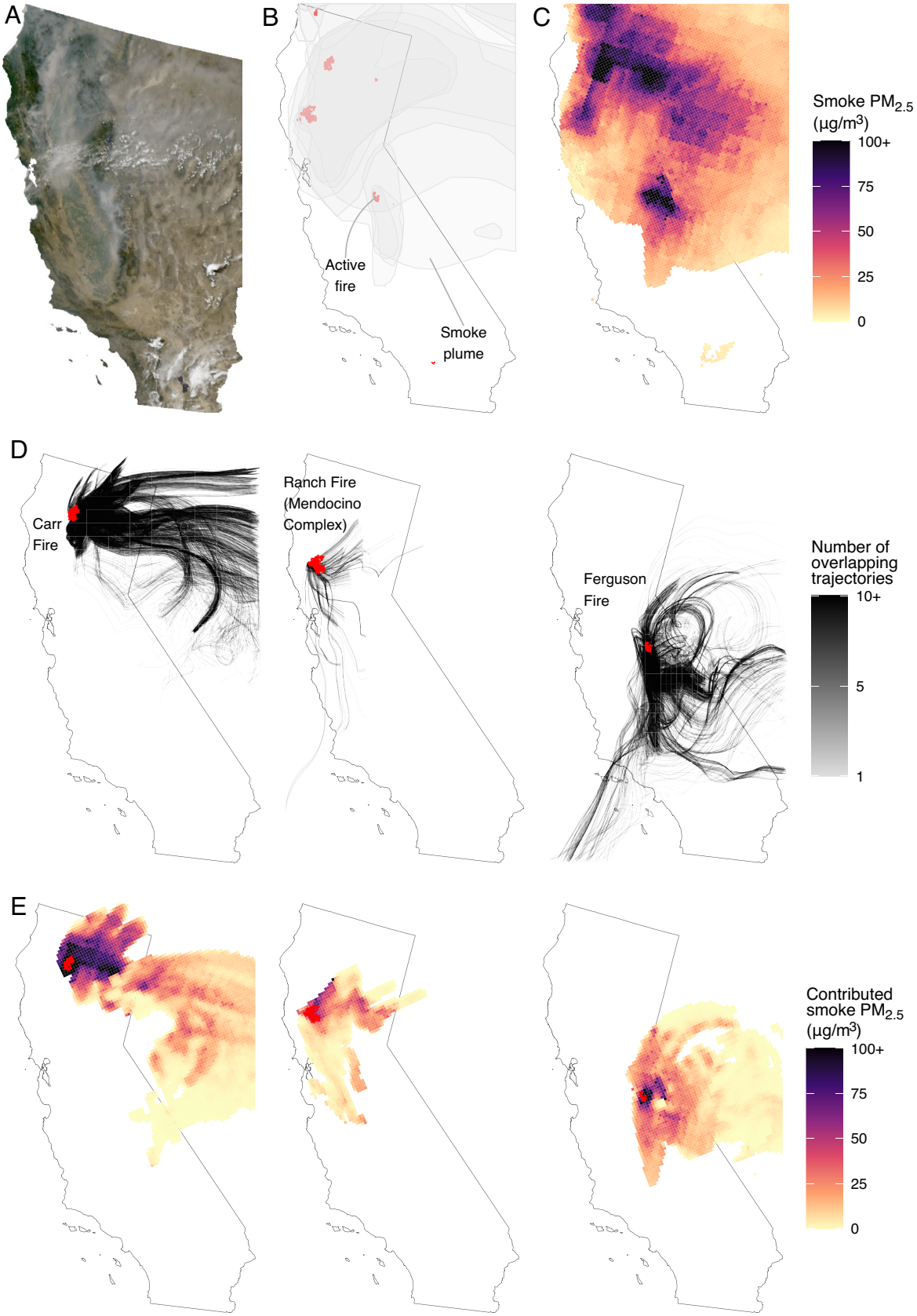

Fig. 1. Attributing wildfire smoke $PM_{2.5}$ to source fires, using active fires in CA on July 29th, 2018, as an example. (*A*) Geostationary satellite imagery over California with visible smoke downloaded from the Registry of Open Data on Amazon Web Services (AWS) (34). (*B*) Hazard Mapping System smoke plume annotations shown in gray. Active fires are shown as red polygons. (*C*) Wildfire smoke $PM_{2.5}$ from all fires with smoke $PM_{2.5}$ capped at 100 μg/m^3, using data from ref. 6. (*D*) HYSPLIT trajectories for three main active fires on July 29th. Each path represents the movement of a particle that originated within the fire polygon up to 5 d before July 29th. Darker paths suggest that more particles followed that trajectory. (*E*) July 29th snapshot of the estimated contribution of each fire to smoke $PM_{2.5}$.

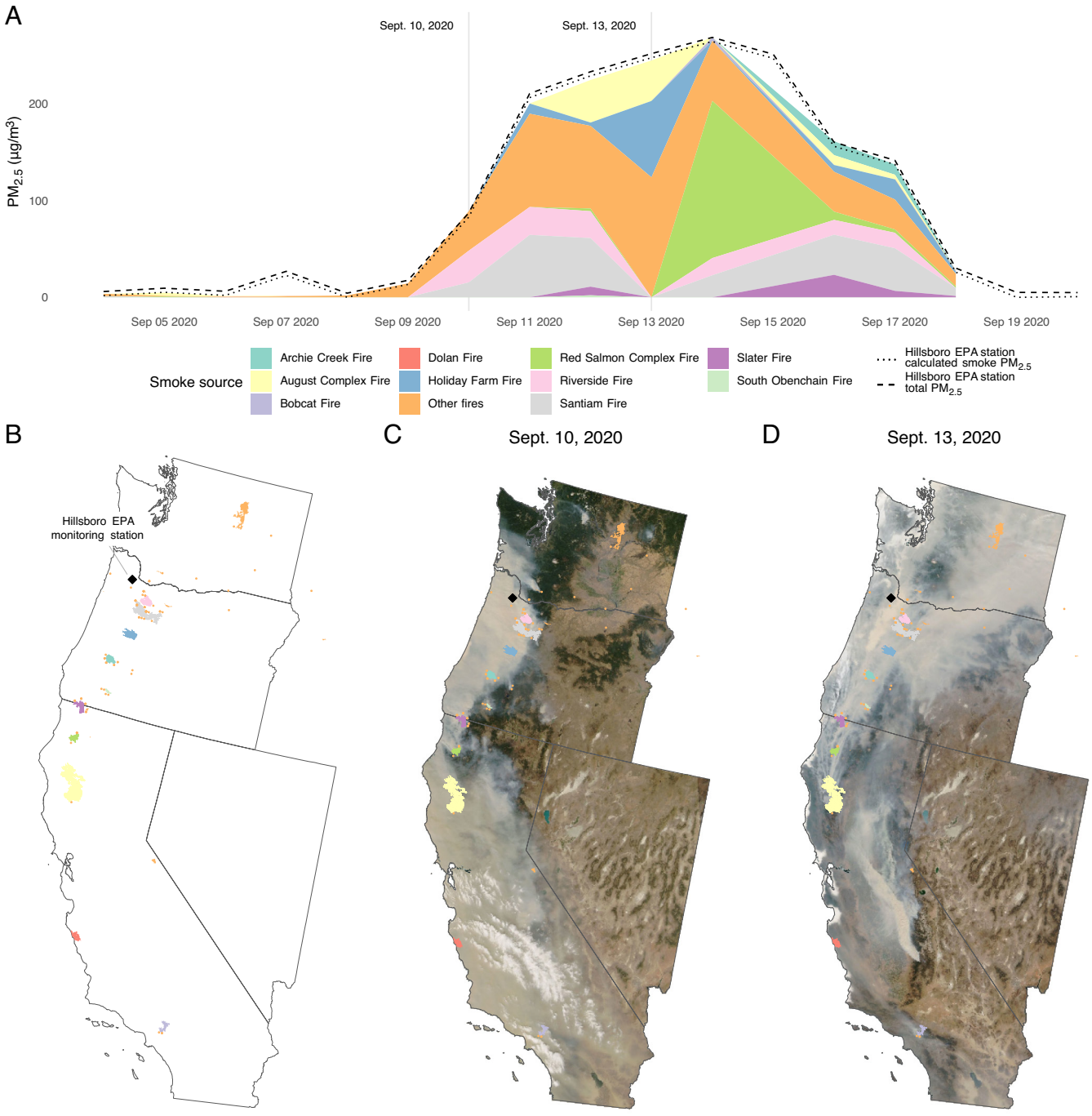

Fig. 2. Fire-specific contributions to Hillsboro EPA monitoring station readings. (*A*) Time-series readings from the Hillsboro EPA air pollution monitoring station show close alignment between the estimated contributed smoke $PM_{2.5}$ from source fires, the "calculated smoke $PM_{2.5}$", and the total $PM_{2.5}$ estimated at the monitoring station. The calculated smoke $PM_{2.5}$ was used in the training process of the smoke $PM_{2.5}$ product in ref. 6. and is estimated at the EPA station by subtracting the month-specific 3-y nonsmoke day median from the total $PM_{2.5}$ readings. The sum of the contributed smoke $PM_{2.5}$ aligns closely with the calculated smoke $PM_{2.5}$ because the machine learning model was trained to predict this value. We direct interest readers to ref. 6. for more information. (*B–D*) Satellite imagery on specific days marked by the dotted vertical lines in panel *A*. Imagery was downloaded from NASA's Worldview application (https://worldview.earthdata.nasa.gov), part of NASA's Earth Observing System Data and Information System (EOSDIS) (35).

has a moderate positive rank correlation with burned area, one of the most commonly used measures of fire activity and severity. We estimate that natural log burned area from each fire and the number of excess asthma ED visits we attributed to each fire has a Spearman rank correlation coefficient of $\rho = 0.29$ (Fig. 4*A*). While there are few very large fires with a small number of attributed asthma ED visits, we see a substantial number of relatively small fires with a high number of excess asthma ED visits, indicating that fire size is only moderately correlated with the population impacts of the fire's smoke. We see similar moderate positive relationship between expenditure on fire suppression and the number of structures destroyed on the number of excess asthma ED visits (Fig. 4 *B* and *C*). Regarding fire suppression, while the fires that resulted in the largest asthma ED visit impacts were those that tended to receive the most suppression resources (Fig. 4 *B*, *Upper Right Corner*), we document a substantial number of fires where the calculated

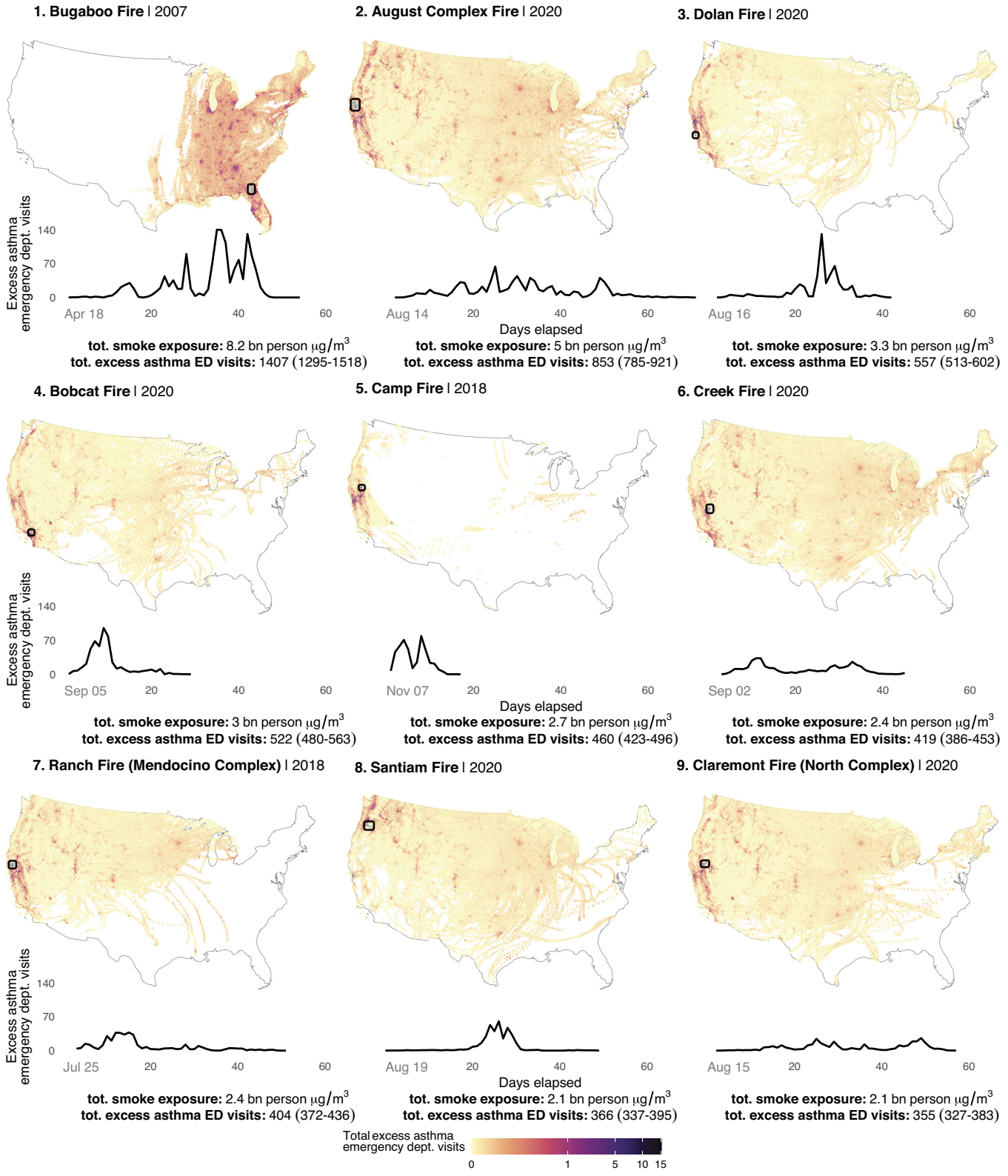

Fig. 3. Top fires ranked by number of estimated attributable excess asthma ED visits from April 2006 to 2020. Each small multiple map shows the total health impacts measured by the number of excess asthma ED visits from wildfire smoke $PM_{2.5}$ aggregated over the duration of the fire (with 95% confidence interval in parentheses). This estimate considers the amount of smoke $PM_{2.5}$, the population affected, and the total number of days of smoke exposure. The line chart shows the estimated asthma-related ED visits from smoke $PM_{2.5}$ over time from the initial day of the fire. Initial fire locations are cyan colored and outlined in black.

number of excess asthma ED visits was high but suppression efforts were modest (points in *Upper Left*), and a similarly high number where suppression costs were high but smoke impacts modest (*Lower Right*). Consistent with this relationship and with the recent finding that fire suppression costs are overwhelmingly determined by the threat of fires to physical structures (38), we find that smoke impact as measured by asthma ED visits only moderately tracked structure damage.

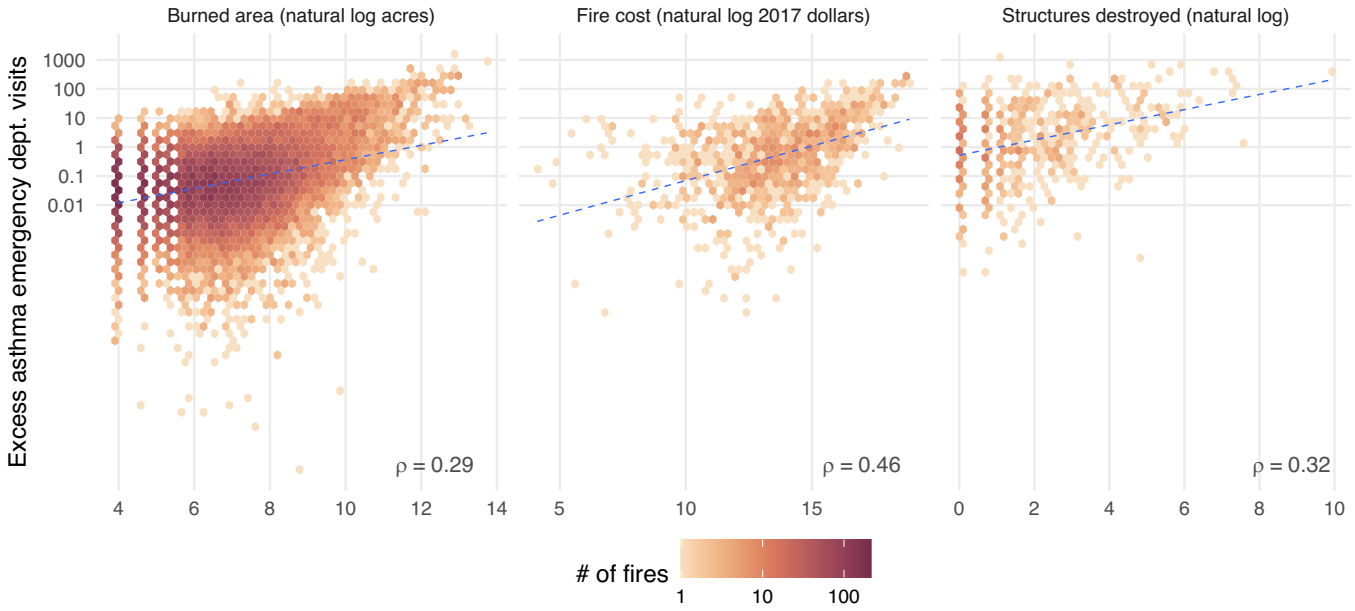

Fig. 4. Comparison between common fire-related severity metrics and attributed excess asthma ED visits. From *Left* to *Right*, the panels show the relationship between the natural log of burned area (acres), fire suppression cost (2017 dollars), or structures destroyed (# structures) vs. the number of excess asthma ED visits from smoke $PM_{2.5}$ with the color of the hexbin indicating the count of individual fires. In the *Left* plot, the burned area is calculated from the GlobFire dataset for fires from April 2006 to 2020 (n = 18,606). For the center plot, only fires greater than 300 acres burned from April 2006 to 2016 in the Western United States are shown due to inconsistent fire suppression cost data for smaller fires and the limited time frame of the fire cost source dataset (n = 984). The *Right* plot shows available data on destroyed structures data for the contiguous United States from April 2006 to 2020 (n = 558). The blue dotted lines represent the fitted regression lines.

We use our linked fire-smoke estimates to quantify the changing overall burden of smoke exposure, to locate the main sources of this exposure, and to characterize the transboundary nature of overall exposure. The magnitude of smoke $PM_{2.5}$ associated number of excess asthma ED visits that the US population experienced doubled from the early less smokey period in 2006 to 2010 to the more smokey late period in 2016 to 2020 (Fig. 5*A*). California was by far the largest source and recipient of wildfire smoke in both periods, with the contribution of CA-sourced smoke to total excess asthma ED visits growing from 26% in the early period to 40% in the late period. While multiple states in the Midwest, South, and East were in the top-5 smoke recipients prior to 2010, a ranking driven in part by large populations in those states, the recent rapid increase in fire activity in the West has meant that Western states now bear a much larger share of the accumulated smoke exposure, sourced from themselves or nearby states.

On average across the United States over our study period, we calculate that 87% of smoke $PM_{2.5}$ comes from "trans-county" sources (i.e., source fires outside the county where the smoke was experienced) and 60% from trans-state sources. In many states, a large portion of smoke $PM_{2.5}$ remains within state borders, but Western US states, such as California, Idaho, and Montana, contribute large amounts of smoke $PM_{2.5}$ to neighboring states (*SI Appendix*, Fig. S7). For recipients of this smoke, large percentages of smoke exposure (e.g., 94% in Nevada) come from out-of-state. Regarding international smoke transport, we find that the share of overall number of excess asthma ED visits experienced in the United States attributable to fires in Canada and Mexico has held steady in both periods at around 8% and 3%, respectively, suggesting that a large proportion (nearly 90%) of smoke exposure in the United States comes from domestic fires.

Using independent gridded estimates of total $PM_{2.5}$ (32), we quantify the contribution of transboundary wildfire smoke $PM_{2.5}$ to total $PM_{2.5}$ between the early (2006 to 2010) and late (2016 to 2020) periods. We find that all counties in the Western United States (414 counties) experienced an increase in the proportion of total $PM_{2.5}$ from out-of-county fire sources (Fig. 5*B*). This finding aligns with literature suggesting that wildfire smoke has slowed, and in some cases reversed, trends in overall air quality improvement (7, 39, 40) and links these reversals to transboundary out-of-county fire sources. In the later period, we calculate that for 120 counties, over a quarter of total $PM_{2.5}$ experienced (sum of daily $PM_{2.5}$ over the 2016 to 2020 period) in that county was from trans-county smoke sources (there were no such counties in the early period) and in 3 counties, over half of total $PM_{2.5}$ was from trans-county smoke sources.

Discussion

Our study develops a method for measuring wildfire impact by connecting individual wildfires to the surface smoke $PM_{2.5}$ that is generated and quantifying the expected number of excess asthma-related ED visits in populations downwind of each fire. Compared to existing efforts that aim to link smoke to fire sources, our method provides granular fire-specific attribution of smoke $PM_{2.5}$ and health impacts at highly resolved temporal and spatial resolution, over the contiguous United States from 2006 to 2020. Existing literature has used the HYSPLIT model (28) to understand smoke transport, but focused on regional transport of smoke rather than specific fire transport and also did not quantify the attributed smoke $PM_{2.5}$. Recent research has used other simplified Lagrangian particle transport models (41) to produce back trajectories of simulated air parcels arriving at specific locations and provide estimates of $PM_{2.5}$ from wildfire smoke. However, this analysis focused on summer months and only conducted population smoke $PM_{2.5}$ analysis for 33 population centers, as compared to our analysis which extends beyond the summer months and covers the contiguous US. The relatively coarse resolution of these analyses' source regions makes it challenging to consider the impact from specific fires.

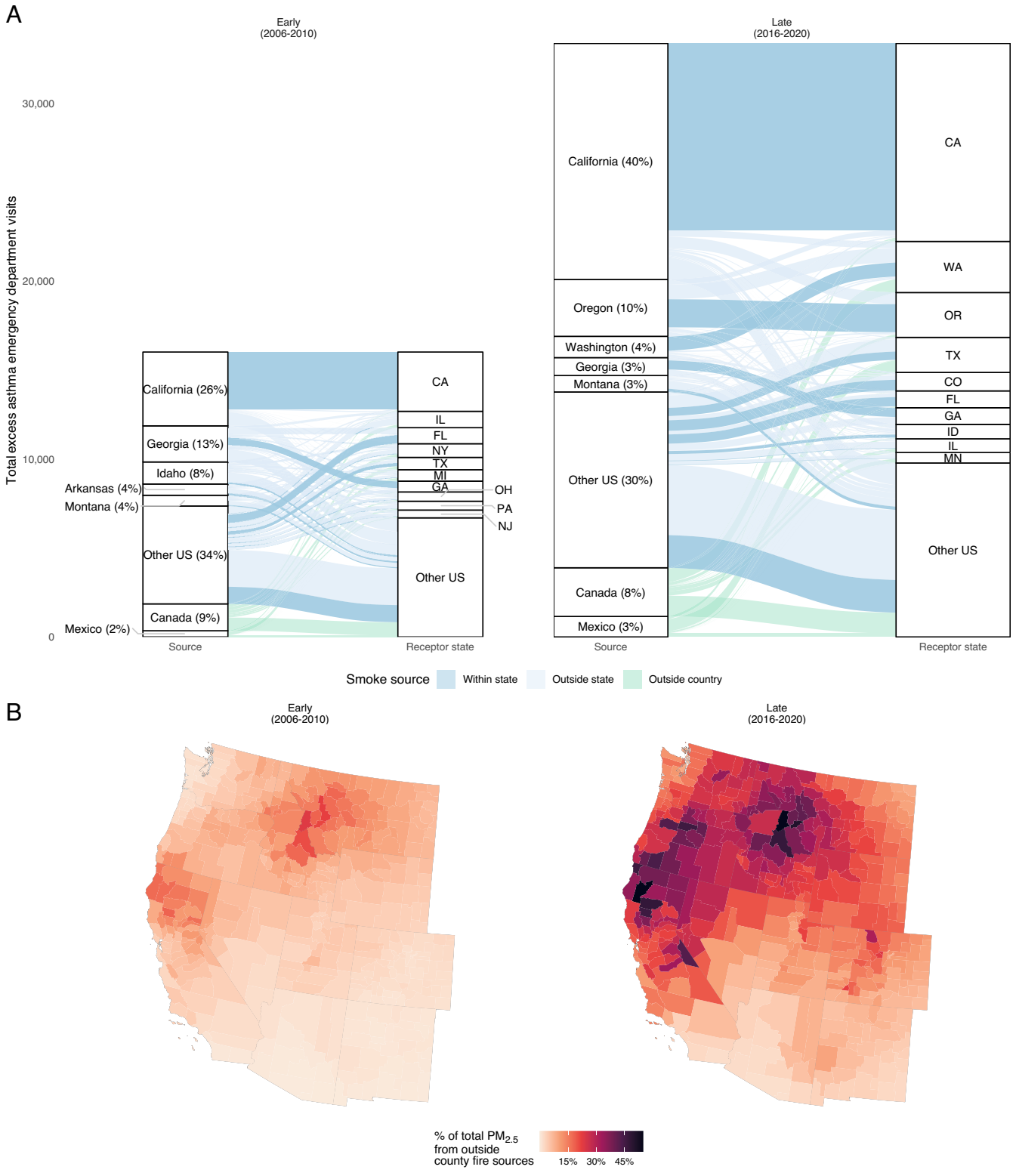

Fig. 5. Interstate transport of smoke $PM_{2.5}$ and contribution of transboundary smoke to total $PM_{2.5}$ concentrations. (*A*) Alluvial diagram of smoke $PM_{2.5}$ from source to receptor states in the early (2006 to 2010) and late (2016 to 2020) periods. Percentages represent the % of total excess asthma ED visits from smoke $PM_{2.5}$ contributed by that state. The dark blue flows represent within state, light blue outside state, and green flows outside country transport of smoke $PM_{2.5}$. (*B*) The fraction of total $PM_{2.5}$ from source fires that are outside of the county in the early (2006 to 2010) and late (2016 to 2020) periods has grown dramatically, especially across the Pacific Northwest, California, Idaho, and Montana.

Other researchers have used a combination of chemical transport models (CTMs) (42), simplified transport models (43), and close proximity air pollution monitors (44) to study the impact of individual wildfires on ambient air quality. However, these studies have primarily only considered the impact of active fires on a relatively small spatial area and the analyses do not cover multiple fires and years. In our work, we consider all smoke-producing fires identified by satellite imagery and trained analysts (6) from April

2006 to 2020. Although CTMs are commonly used to estimate the impact of specific air pollutants on downwind communities (45–47), uncertainty around surface fuel characteristics and emission inventories result in highly variable estimates of PM air pollution from fires (48, 49). Additionally, the computational burden of running these models limits their applicability in our context, as comprehensive characterization of smoke contributions would require a separate model run for each of the fires in our data. Related studies that use satellite imagery or surface observations to analyze air pollution trends in the Western United States (6, 11, 50, 51) provide insight into the overall contribution of wildfire to regional air quality trends but are unable to link smoke to specific source fires.

We estimate health-related smoke impacts due to smoke $PM_{2.5}$ by applying previously calculated relationships between smoke $PM_{2.5}$ and asthma-related ED visits. Our approach follows existing literature on the health impacts of smoke and assumes that the asthma-related impacts of smoke are a linear function of accumulated daily exposure (31, 52) and that different income/ demographic subgroups respond similarly to the same level of smoke exposure (53) (*SI Appendix*, Fig. S8). We note that the use of any other health concentration–response function that is also linear [e.g., smoke-mortality (36)] in our framework would generate the same health impact ranking for fires. However, even if health outcomes in different communities respond similarly to a given change in smoke exposure, there is substantial variation in the total amount of smoke that different communities are exposed to, either from specific fires or from wildfires as a whole, with Hispanic and Native communities often exposed at much higher levels (6). By counting total excess asthma-related ED visits, our estimates could obscure acute impacts among groups with smaller populations but high exposure levels. Understanding fire-specific impacts on specific vulnerable subgroups of interest is an important area for future work. Similarly, in the absence of a nationally representative estimate of smoke-asthma concentration–response function, we rely on recent evidence from CA (31, 53). While CA is a state with large variation in smoke exposure and rich socioeconomic and demographic diversity, we hope that future work can estimate rigorous, nationally representative health response functions that can be applied in this sort of analysis. More broadly, our approach could account for different health outcomes, nonlinear mappings of exposure to health impacts, differential impacts across income or other demographic characteristics, or heterogeneous impacts by location if future data support such revisions.

Our analysis identifies the Bugaboo Scrub Fire in 2007 as producing the highest number of excess asthma ED visits during our study period. One reason for the high impact of this fire is its proximity to large urban areas and that smoke from this fire transported across much of the Eastern Seaboard (*SI Appendix*, Fig. S6). Recent research also suggests that slower-burning smoldering fires, similar to the peatland fires in the Bugaboo fire, could release large amounts of harmful PM due to incomplete combustion of surface matter, which ultimately results in high smoke $PM_{2.5}$ emissions (49, 54). Better understanding the landscape features that predict smoke emissions is an active and important area for additional work. While the Bugaboo fire could have truly been more smoke-producing than other fires, we note that the fire had a higher attribution certainty (score of 89%) compared to other top fires, such as the 2020 California fires (attribution certainty scores around 50%) suggesting greater uncertainty around the smoke $PM_{2.5}$ of the 2020 California fires because multiple other fires were occurring at the same time and contributing smoke to the same locations (*SI Appendix*, Table S1).

The moderate correlation between the number of excess asthma ED visits and other common measures of fire severity is consistent with the large observed share of suppression resources spent on limiting physical property damage (38, 55). Fires that threaten structures in less densely populated wildland–urban interface regions are often more expensive to suppress (38), but often result in smaller population exposure to smoke. On the other hand, fires further from populated areas may threaten fewer structures and receive less suppression effort but can generate large amounts of smoke that have more distant but likely very large health impacts, including increased mortality. We emphasize that our results do not necessarily imply that more suppression resources should be directed toward fires that generate large smoke impacts. Wildfire suppression decisions often involve complex sets of objectives and constraints, such as managing a fire to support natural ecosystem and wildlife habitat development or reducing the risk of harmful toxic smoke from burned structures (22), in addition to protecting the structures themselves, under significant time pressure. However, conditional on using fire suppression to manage societal risk, further recognition and quantification of downwind smoke impacts may help inform and shift future resource allocation decisions (19). Other management actions such as increased investment in the use of low-intensity fires could both reduce the risks of wildfires and the quantity and impacts of smoke that is generated (18–20). We also note that while our analysis provides a retrospective analysis of smoke impacts, future wildfire management decisions would require additional research and improvements in medium and long-term forecasts of smoke dispersion and impacts.

Our smoke-linking method is able to capture a majority of smoke $PM_{2.5}$ contributed by specific fires, as shown by analysis of isolated fires where our method captures most but not all of nearby smoke (*SI Appendix*, Figs. S2 and S3). Nevertheless, attributions are limited in part by analysts' abilities to identify smoke-producing fire points, from which HYSPLIT trajectories are initialized, and our ability to accurately match fire points to fire polygons. Future work that leverages satellite sensors with higher spatial and temporal resolution could improve the identification of smoke-producing fires and/or active fire-burned areas and refine the fire ignition point to fire polygon match. Further refinements to the smoke $PM_{2.5}$ attribution function could also result in better estimates of fire-specific smoke $PM_{2.5}$. Specifically, while our approach allows us to calculate the average age of particles belonging to a fire, we do not use this information to attribute smoke $PM_{2.5}$ to fires. Future research that sheds light on how age of smoke modulates PM concentration and composition can be used to improve the attribution function and/or estimates of health impacts. Our analysis could also potentially misattribute diffuse smoke with longer atmospheric residence time because we model HYSPLIT trajectories for 6 d after the fire ignites (*Methods*). After this period, the smoke could remain in the atmosphere, but we would not be able to associate it with a source fire. Then, if another fire generates smoke trajectories that intersect with this old smoke, the smoke would be assigned to the new fire. Extending the HYSPLIT modeling to account for long-lasting smoke could help reduce this occurrence.

Improved estimates of smoke plume injection height could also lead to better modeling of smoke transport, as literature suggests that the injection height of smoke plumes plays a large role in smoke transport but that accurate estimates of fire-specific injection heights are limited (49). While the majority of observed wildfire smoke injection occurs at near-surface altitudes (below 2,000 m above ground), some intense fires in the summer months can loft smoke to higher altitudes (56). To account for uncertainty

in the injection height of plumes and following previous literature (28), we initialize trajectories at 3 different injection heights (500, 1,500, and 2,500 m above ground level) for each fire and use the 3 initialized trajectories evenly for all fires (*Methods*). Although this approach allows us to cover the range of historically observed smoke injection heights and weight toward near-surface injection, when there are multiple overlapping plumes, it could result in overestimation of distant smoke $PM_{2.5}$ for smaller, cooler fires that are likely to have lower injection heights. Local smoke $PM_{2.5}$ can also be overestimated for larger, hotter fires as these fires tend to have higher injection heights that travel greater distances. Recent satellite-derived estimations of smoke injection heights can further constrain the smoke injection height and lead to better trajectory modeling, but this approach is challenging due to the high proportion of missing observations in wildfire smoke-saturated areas (57). However, leveraging further developments in satellite observation derived or modeled smoke plume injections could result in more accurate trajectories (58).

We use high-resolution predictions of daily smoke $PM_{2.5}$ (6) across the contiguous United States to determine the surface-level smoke associated with fires. These estimates were generated by training a machine learning model to predict daily smoke $PM_{2.5}$ from a combination of satellite, reanalysis, and air trajectory simulations. Limitations of this upstream product will affect the results of this study. Specifically, the authors note that while the predicted product has an overall spatial out-of-sample model performance of R^2 = 0.67 (with 90% of held-out EPA monitoring station-specific R^2 values between 0.21 and 0.88), the model struggles in certain geographies, such as the Southwest, and in situations when smoke appears overhead but does not mix to the surface. In these instances, the attributed smoke exposure and health impacts would also be less accurate.

Our method links smoke $PM_{2.5}$ to source fires, which enables further analysis to better understand how fire characteristics might drive differential smoke toxicity. Recent literature suggests that wildfires can convert and release toxic elements, such as hexavalent chromium, into the atmosphere, but analysis has been limited to specific study sites (59). This work provides an approach to more broadly investigate whether burning specific materials, such as man-made structures (60), or other fire characteristics, such as smoke age, results in different smoke air pollution toxicity. We note that smoke particles that travel long distances can react and become more toxic when exposed to sunlight and other atmospheric chemicals (61). Our approach does not model the chemical processes of these reactions.

As the climate continues to warm and wildfires increase across much of the Western United States and beyond (1, 62), PM air pollution from these events is trending upward and expected to worsen in the coming decades (5–7, 63). A growing literature finds that exposure to wildfire smoke results in a range of negative societal impacts, including impacts on respiratory-related morbidity and all-cause mortality (12, 52, 64), interrupted learning (17, 65), and decreased labor productivity (66). Our work provides a method to connect these smoke $PM_{2.5}$ impacts back to specific source fires and can help clarify policy options that aim to better allocate resources to address this growing environmental challenge.

Methods

HYSPLIT Trajectories for Smoke-Producing Fires. In this work, we leverage the HYSPLIT model (67) to track the movement of smoke emitted from particular fires and to allocate $PM_{2.5}$ surfaces back to source fires. These data represent simulated forward trajectories of smoke particles emitted at smoke-producing fire points (HYSPLIT points) for all automatically detected and manually added fire hotspots identified by trained Hazard Mapping System (HMS) analysts (28, 68) between April 2006 and December 2020. The satellite-detected fire points are validated and identified as smoke-producing by HMS analysts and false positives are removed to generate a set of HYSPLIT initialization points, from which forward trajectories are run [see supplemental information of Childs et al. (6) for details of trajectory generation]. To incorporate uncertainty about smoke injection heights, we follow previous literature (28) and initialize three trajectories at each point beginning at different altitudes (500, 1,500, and 2,500 m above ground level) and use the generated trajectories evenly for all fires.

In total, there are 2.4 million distinct HYSPLIT initialization points from April 2006 to December 2020 that each have three associated 6 d trajectories (one for each initial altitude). Each trajectory is defined as a sequence of estimated latitude, longitude, and height coordinates at hourly time steps following initialization. For each trajectory, we calculate the cumulative rainfall and minimum height so far on the trajectory path. We truncate each trajectory path by removing trajectory points that have been rained out or that have collided with the ground. With the remaining trajectory points, we calculate the cumulative trajectory distance from the fire polygon centroid or initial HYSPLIT point (if the initialization point did not fall within any fire polygons) to each successive point on the trajectory path, which we later use to distribute smoke $PM_{2.5}$. For each HYSPLIT initialization point, HMS analysts assign a "duration" value that represents the number of hours that the specific fire produces smoke and analysts may duplicate fire points to represent severe smoke-producing fires. We run trajectories over the duration of each fire and remove duplicated fire points to reduce computation. After generating fire trajectories, we weigh each initialization point to account for the duplicated fire points that had been identified for that initialization time.

Assigning HYSPLIT Initialization Points to Fires. To group HYSPLIT initialization points, which are not associated with specific named fires, belonging to the same source fire, we match the location of HYSPLIT initialization points to a separate database of known fires. We use fire boundary shapes from the GlobFire v3 dataset subsetted to North America from April 2006 to 2020 (69). These fire polygons represent the final area of fires detected by NASA's MODIS satellite and provide a single polygon of the total burned area for each detected fire with start and end dates. After matching the fire polygons with the locations of the smoke-producing HYSPLIT initialization points, we filter for points that fall between the start and end dates of the fire polygons. The resulting matched dataset represents the fire polygons and associated smoke-producing fire points.

Because a large number of HYSPLIT initialization points are satellite derived, the accuracy of the fire location is dependent on the resolution of the satellite product used to identify these fires and recent literature has suggested that the accuracy of HYSPLIT initialization points is around 2 to 3-km (28). As shown in *SI Appendix*, Fig. S9, the HYSPLIT initialization points, which are partially algorithmically identified as thermal hotspots, appear to follow a rectangular grid and result in some smoke-producing HYSPLIT initialization points that fall outside of the buffered fire polygon. These points likely belong to the fire as there are no other fires nearby at this time and could contribute to decreased attribution of contributed smoke $PM_{2.5}$ to this specific fire. Aligned with recent research that has shown a 2-km median spatial offset between the MODIS burned area product and identified fire points (70), we add a 2-km buffer to the boundary of detected fire polygons to account for this potential resolution-based inaccuracy. A larger buffer around the fire polygon would lead to more associated HYSPLIT initialization points per fire and therefore potentially larger smoke exposure and excess asthma ED visit estimates, at the potential cost of associating HYSPLIT initialization points with the wrong fire. We take the conservative approach and use a 2-km buffer, as suggested by the literature.

About 65% (1546271/2372751) of the nearly 2.4 million HYSPLIT initialization points (smoke-producing fires) are matched to a fire polygon with a majority of the unmatched HYSPLIT initialization points occurring in recent years (*SI Appendix*, Fig. S10). One potential reason for more unmatched fire points in recent years is the inclusion of the hotspot detections from the Visible Infrared Imaging Radiometer Suite sensor starting in 2016, which has a higher resolution and detects more thermal anomalies (71) than previous thermal sensors used by the HMS system. To ensure that we do not ignore the smoke generated from the unmatched HYSPLIT initialization points, we assume that if a HYSPLIT initialization point does not fall into a buffered fire polygon, then it is a separate fire.

Calculating Smoke $PM_{2.5}$ from Specific Fires. To estimate the contribution of smoke $PM_{2.5}$ from specific fires, we combine the fire polygon matched trajectories with previous estimates of daily 10-km all-fire smoke $PM_{2.5}$ over the period from April 2006 to 2020 (6). We first match trajectory points to 10-km gridcells using the trajectories described above for all of North America from April 2006 to 2020. After linking trajectory points (and initial source fire) to overlapping gridcells, we use a window function (spatial buffer) to account for the spatial dispersion of smoke particulates, as trajectory points represent a single point estimate of the likely location that an air parcel traveled. In reality, smoke could disperse and affect a larger area. We considered different window sizes ranging from no buffering around the gridcell where a trajectory point landed (just consider the 10-km gridcell where a trajectory point landed), all immediately neighboring gridcells (effectively a 30-km window centered on the gridcell where a trajectory point landed), and two rings of neighboring 10-km gridcells (a 50-km window centered on the gridcell where the trajectory point landed). We find that the 10-km window potentially underestimates the amount of fire-specific smoke $PM_{2.5}$ leaving on average over 60% of all-fire smoke $PM_{2.5}$ unaccounted for (*SI Appendix*, Fig. S11). We conduct the analysis with the 30-km window, which is more conservative than the 50-km window but makes up for a large portion of the all-fire smoke $PM_{2.5}$ that the 10-km window misses.

Although we are able to calculate the height of HYSPLIT trajectory points, we do not currently use this information (besides filtering out points that have been rained-out or that have collided with the ground) to distribute the smoke $PM_{2.5}$ to specific fires. To distribute all-fire smoke $PM_{2.5}$ at the gridcell to individual fires, we consider the number of trajectory points and cumulative trajectory distance of those points from a source fire. Specifically, as shown in *SI Appendix*, Fig. S1, for an individual gridcell, we first calculate the denominator total gridcell weight as the sum of inverse distance weighted trajectory point counts. In the supplemental figure example of the multiple fire, there are 5 trajectory points in gridcell 3 with 2 belonging to fire A and 3 belonging to fire B. Each of these trajectory points has a cumulative trajectory distance. The total gridcell weight is the sum of these inverse cumulative trajectory distances. This simplified example does not consider the spatial buffer described above, but the 30-km spatial buffer used in the main analysis would work similarly and also count trajectory points in the neighboring ring of gridcells. After calculating this total gridcell weight, we calculate a fire-specific gridcell share, which sums the inverse distance weighted trajectory counts from a specific fire and normalizes the value by the total gridcell weight. In *SI Appendix*, Fig. S1, fire A is calculated to have 10% share of all-fire smoke $PM_{2.5}$ in gridcell 3 and fire B accounts for the remaining 90% share of all-fire smoke $PM_{2.5}$ in the gridcell. The calculation of smoke $PM_{2.5}$ from a single fire is the same as in the multiple fire case; however, because there are no trajectory points from other fires the calculated share for the single fire is 100%. Lastly, to distribute the all-fire smoke $PM_{2.5}$ in a specific gridcell to individual fires, we multiply the fire-specific share with the total all-fire smoke $PM_{2.5}$ in the gridcell.

Estimating Population Smoke Exposure in Each Gridcell. We estimate the population impacted by smoke $PM_{2.5}$ from specific fires by combining the wildfire attributed smoke $PM_{2.5}$ with gridded population data from WorldPop (72). We use the unconstrained individual countries 2000 to 2020 UN adjusted (1-km resolution) dataset (https://hub.worldpop.org/doi/10.5258/SOTON/WP00671) and download data for the United States. We first calculate the yearly population in 10-km gridcells aligning with our smoke $PM_{2.5}$ grid by taking an area-weighted sum of the 1-km WorldPop grid cells that fall into our 10-km smoke $PM_{2.5}$ grid across the contiguous United States from 2006 to 2020. Then, to calculate the daily smoke exposure at the gridcell, we multiply the fire-specific contributed smoke $PM_{2.5}$ with the population at the gridcell. In *SI Appendix*, Fig. S1, for the multiple fire case, gridcell 3 has a population of 10 so the smoke exposure from fire A is the product of fire A's share, the total smoke $PM_{2.5}$, and the population in the gridcell, which equals 20 person $\mu g/m^3$. Smoke exposure for fire B follows a similar calculation and is estimated to have 180 person $\mu g/m^3$ of smoke exposure. To calculate the smoke exposure for an individual fire over the duration of the fire, we sum the daily smoke exposure across gridcells and days.

Calculating Number of Excess Asthma ED Visits. To estimate health impacts of population smoke exposure from each fire, we build on recent work in CA (31) that linked estimates of smoke $PM_{2.5}$ to georeferenced data on ED visits from 2006 to 2017 in the state. Using the same data (73) and a similar empirical framework, we derive diagnosis specific zipcode by day ED visit rates and estimate how zipcode-level ED visits for asthma (one of the most well-established health impacts associated with wildfire smoke) respond to variation in wildfire smoke $PM_{2.5}$ concentrations in that zip code. On average there are 1.17 daily ED visits per 100 K for asthma in our sample. To estimate an appropriate response function that can be applied to the current setting, we first assess whether the number of ED visits for asthma (1) responds linearly to wildfire smoke and (2) differs across income groups. Specifically, we estimate the following panel fixed effects regression:

$$y_{zcdw} = \sum_{l=0}^{7} \beta_l f\left(smoke_{z,d-l}\right) + \alpha X_{zcdw} + \delta_z + \theta_{cm} + \eta_{sy} + \omega_w + \varepsilon_{zcdw}, \quad [1]$$

where y_{zcdw} is the daily rate of ED visits for asthma in zipcode z, county c, date d, day-of-week w where the date falls into month m, season s, and year y. $smoke_{z,d-l}$ is the smoke $PM_{2.5}$ concentration (6) at the zipcode by day level. Because some ED visits are likely to occur not on the same day of exposure but in the following days, we estimate a distributed lag model with multiple daily lags (l). To account for any time-invariant differences across locations in average smoke exposure or average ED visitation, local seasonality in smoke or ED visitation, state-wide time trends in either variable, and within-week variation in ED visitation patterns, we include zipcode (δ_z), county by month-of-year (θ_{cm}), season-by-year (η_{sy}), and day-of-week (ω_w) fixed effects, respectively. Based on previous work (31), we include 7 d of lagged smoke $PM_{2.5}$ (i.e., day-of-exposure and an additional week of daily lags) and calculate the cumulative effect of a smoke $PM_{2.5}$ by summing β_l values across lags and calculating the analytical SEs for these sums. SEs are also clustered at the zipcode level.

In Eq. **1**, the effect of wildfire smoke visits is identified using within-location variation in smoke exposure over time. In essence, it compares ED visits in a given location on smokey vs. less smokey (or smokeless) days, and asks whether ED visits are higher on days when smoke is in the air, accounting for anything that affects ED visits or smoke concentrations in a common way across locations (e.g., long term increases in ED visits, or short-term shocks from a bad flu season), anything that affects local-level ED visits or smoke in a seasonal way (e.g., wintertime ED visit average visits are higher in Fresno than in San Francisco, summertime smoke is higher in Sacramento than Los Angeles), and any differences on average across days in the week (e.g., weekends have higher ED visits that weekdays). Because the remaining local-level temporal variation in smoke is highly random, driven by idiosyncrasies in where and when fires start and how the wind blows on a given day, we believe that it is unlikely correlated with any other remaining unobserved factor also correlated with ED visits.

To assess linearity of the estimated response, we estimate separate versions of Eq. **1** where $f(smoke_{zcw,d-l})$ takes either linear or quadratic functional forms. In doing so, we find little difference between the estimated linear and quadratic responses (*SI Appendix*, Fig. S8*A*). This linearity is consistent with other estimates in the literature that also estimate (or assume) linear relationships between respiratory, cardiovascular, and mortality-related outcomes and of wildfire smoke exposure (36). To assess whether impacts differ by income group we therefore utilize the linear version of Eq. **1** and interact the smoke $PM_{2.5}$ terms with zipcode level average median income terciles. We find small differences between groups that are not statistically different from each other (*SI Appendix*, Fig. S8*B*).

Given this linear relationship that appears to be similar across income groups, we calculate excess asthma ED visits for each gridcell-day by directly multiplying the gridcell level smoke exposure (fire-specific contributed smoke $PM_{2.5}$ multiplied by the gridcell population) by the estimated effect of smoke $PM_{2.5}$ on excess asthma ED visit rates. We then estimate the total number of asthma ED visit health impacts from a specific fire by summing across the gridcell estimates of excess asthma ED visits over the duration of the fire. We estimate 95% CIs on fire-specific attributed asthma ED visits by using the SEs estimated in the asthma concentration–response function (Eq. **1**), multiplying by the population smoke exposure, and then summing up across gridcells for the duration of the fire.

This approach to calculating excess ED visits assumes that the response estimated from asthma ED visits in California applies to other states. While we cannot directly assess this assumption, we select asthma ED visits as our example health outcome of interest for this exercise in part because it has been extensively linked to wildfire smoke in a wide variety of settings (3). The substitution of any other linear wildfire-health dose–response function that measures outcomes in rates will yield a similar rank ordering of fire severity as our asthma ranking.

Nonlinear dose–response functions, functions that show heterogeneous effects across demographic subgroups, or functions that measure outcomes as percentage change in rates (when baseline rates differ across populations) could yield different rankings.

Comparison with Fire Suppression Costs and Structures Burned. To estimate the relationship between suppression costs and smoke $PM_{2.5}$ exposure, we use data from Baylis and Boomhower (38), which includes fire suppression costs for fires in 11 Western states from 2006 to 2016. Due to lack of consistent fire suppression cost reporting, we focus analysis on fires larger than 300 acres. The fire-fighting suppression costs are collected from different Freedom of Information Act and public records requests to six federal and state agencies. We direct interested readers to Baylis and Boomhower (38) for additional details. We match the fire suppression cost data to specific fires by identifying observations that fall into buffered (500 m) fire polygons and by ensuring that the ignition date present in the suppression dataset falls within 2 d of the initial start date of the fire polygon. We match the destroyed structures dataset (37) to individual fires in a similar way by filtering to the matching year and finding structure burned locations that fall within the buffered fire polygons.

Calculating Total $PM_{2.5}$ for Transboundary Analysis. In order to compare smoke $PM_{2.5}$ to total $PM_{2.5}$ for counties, we calculate the average daily total $PM_{2.5}$ for each 10-km gridcell in 11 Western States from 2006 to 2020 using data from Swanson et al. (32). We use the exactextractr R package and take the area weighted mean of the 1-km gridcells that fall into the smoke $PM_{2.5}$ 10-km gridcells. We then identify the 10-km gridcells that overlap with counties and sum over the gridcell-days for both smoke $PM_{2.5}$ and total $PM_{2.5}$. Using the location of the source fire and the amount of contributed smoke $PM_{2.5}$ in each gridcell, we can calculate the proportion of total $PM_{2.5}$ in each gridcell that comes from out-of-county source fires.

Calculating Attribution Certainty Score for Each Fire. The fire-specific attribution certainty score estimates the percent of a fire's smoke exposure that happens on days when there is no smoke from other fires. To calculate this score, we take a weighted average of the share of gridcell smoke $PM_{2.5}$ weighting by the smoke exposure of a specific fire. We walk through an example of this calculation for the single vs. multiple fire case in *SI Appendix*, Fig. S4. As described above, the share calculation of a fire takes into account the number of trajectory points and the cumulative trajectory distance of the points that belong to a specific fire divided by the gridcell total weight.

Data, Materials, and Software Availability. The code and data to replicate the results and figures in the main text and *SI Appendix* will be made available upon publication at https://github.com/jeffwen/smoke_linking_public (74).

ACKNOWLEDGMENTS. We thank Jessica Li for help generating HYSPLIT trajectory data, Kimiko Barrett for sharing data on structures burned, and the ECHOLab at Stanford University for helpful discussions. We also thank Stanford University and the Stanford Research Computing Center for providing computational resources that contributed to these research results. M.B. thanks the Robert Wood Johnson Foundation (ID# 76555) and the Stanford Woods Institute Environmental Ventures Project for funding. J.W. gratefully acknowledges funding from Stanford Data Science and The Ram and Vijay Shriram Sustainability Fellowship for this work. J.B. thanks the Carnegie Corporation of New York for support via the Andrew Carnegie Fellowship. The funders had no role in study design, data collection and analysis, decision to publish, or preparation of the manuscript.

Author affiliations: [a]Department of Earth System Science, Stanford University, Stanford, CA 94305; [b]Center on Food Security and the Environment, Stanford University, Stanford, CA 94305; [c]Department of Economics, University of British Columbia, Vancouver, BC V6T 1Z4, Canada; [d]Department of Economics, University of California, San Diego, CA 92093; [e]National Bureau of Economic Research, Cambridge, MA 02138; and [f]Doerr School of Sustainability, Stanford University, Stanford, CA 94305

1. J. T. Abatzoglou, A. P. Williams, Impact of anthropogenic climate change on wildfire across Western US forests. *Proc. Natl. Acad. Sci. U.S.A.* **113**, 11770–11775 (2016).
2. Bonne Ford *et al.*, Future fire impacts on smoke concentrations, visibility, and health in the contiguous United States. *GeoHealth* **2**, 229–247 (2018).
3. C. E. Reid, M. M. Maestas, Wildfire smoke exposure under climate change: Impact on respiratory health of affected communities. *Curr. Opin. Pulm. Med.* **25**, 179 (2019).
4. R. Aguilera, T. Corringham, A. Gershunov, T. Benmarhnia, Wildfire smoke impacts respiratory health more than fine particles from other sources: Observational evidence from Southern California. *Nat. Commun.* **12**, 1–8 (2021).
5. R. R. Buchholz *et al.*, New seasonal pattern of pollution emerges from changing North American wildfires. *Nat. Commun.* **13**, 1–9 (2022).
6. M. L. Childs *et al.*, Daily local-level estimates of ambient wildfire smoke $PM_{2.5}$ for the contiguous US. *Environ. Sci. Technol.* **56**, 13607–13621 (2022).
7. M. Burke *et al.*, The contribution of wildfire to $PM_{2.5}$ trends in the USA. *Nature* **622**, 761–766 (2023).
8. F. Kazemiparkouhi *et al.*, The impact of long-term $PM_{2.5}$ constituents and their sources on specific causes of death in a US medicare cohort. *Environ. Int.* **159**, 106988 (2022).
9. G. D. Thurston *et al.*, Ischemic heart disease mortality and long-term exposure to source-related components of US fine particle air pollution. *Environ. Health Perspect.* **124**, 785–794 (2016).
10. M. d. M. Rahman *et al.*, Cardiovascular morbidity and mortality associations with biomass-and fossil-fuel-combustion fine-particulate-matter exposures in Dhaka, Bangladesh. *Int. J. Epidemiol.* **50**, 1172–1183 (2021).
11. K. O'Dell, B. Ford, E. V. Fischer, J. R. Pierce, Contribution of wildland-fire smoke to US $PM_{2.5}$ and its influence on recent trends. *Environ. Sci. Technol.* **53**, 1797–1804 (2019).
12. C. E. Reid *et al.*, Critical review of health impacts of wildfire smoke exposure. *Environ. Health Perspect.* **124**, 1334–1343 (2016).
13. C. J. L. Murray *et al.*, Global burden of 87 risk factors in 204 countries and territories, 1990–2019: A systematic analysis for the global burden of disease study 2019. *Lancet* **396**, 1223–1249 (2020).
14. M. Abdo *et al.*, Impact of wildfire smoke on adverse pregnancy outcomes in Colorado, 2007–2015. *Int. J. Environ. Res. Public Health* **16**, 3720 (2019).
15. S. Amjad, D. Chojecki, A. Osornio-Vargas, M. B. Ospina, Wildfire exposure during pregnancy and the risk of adverse birth outcomes: A systematic review. *Environ. Int.* **156**, 106644 (2021).
16. S. Heft-Neal, A. Driscoll, W. Yang, G. Shaw, M. Burke, Associations between wildfire smoke exposure during pregnancy and risk of preterm birth in California. *Environ. Res.* **203**, 111872 (2022).
17. J. Wen, M. Burke, Lower test scores from wildfire smoke exposure. *Nat. Sustain.* **5**, 947–955 (2022).
18. M. North, B. M. Collins, S. Stephens, Using fire to increase the scale, benefits, and future maintenance of fuels treatments. *J. Forestry* **110**, 392–401 (2012).
19. D. W. Schweizer, R. Cisneros, Forest fire policy: Change conventional thinking of smoke management to prioritize long-term air quality and public health. *Air Quality, Atmos. Health* **10**, 33–36 (2017).
20. P. F. Hessburg, S. J. Prichard, R. K. Hagmann, N. A. Povak, F. K. Lake, Wildfire and climate change adaptation of western North American forests: A case for intentional management. *Ecol. Appl.* **31**, e02432 (2021).
21. M. P. North *et al.*, Environmental science. Reform forest fire management. *Science* **349**, 1280–1281 (2015).
22. C. A. Schultz, M. P. Thompson, S. M. McCaffrey, Forest service fire management and the elusiveness of change. *Fire Ecol.* **15**, 1–15 (2019).
23. Y. H. Kim *et al.*, Chemistry, lung toxicity and mutagenicity of burn pit smoke-related particulate matter. *Particle Fibre Toxicol.* **18**, 1–18 (2021).
24. L. N. Kobziar *et al.*, Pyroaerobiology: The aerosolization and transport of viable microbial life by wildland fire. *Ecosphere* **9**, e02507 (2018).
25. L. N. Kobziar *et al.*, Wildland fire smoke alters the composition, diversity, and potential atmospheric function of microbial life in the aerobiome. *ISME Commun.* **2**, 1–9 (2022).
26. L. M. David *et al.*, Could the exception become the rule 'uncontrollable' air pollution events in the US due to wildland fires. *Environ. Res. Lett.* **16**, 034029 (2021).
27. Government Accountability Office, Wildfire smoke: Opportunities to strengthen federal efforts to manage growing risks (GAO publication no. GAO-23-104723, U.S. Government Printing Office, Washington, D.C., 2023). https:// www.gao.gov/products/gao-23-104723. Accessed 26 April 2023.
28. S. J. Brey, M. Ruminski, S. A. Atwood, E. V. Fischer, Connecting smoke plumes to sources using hazard mapping system (HMS) smoke and fire location data over North America. *Atmos. Chem. Phys.* **18**, 1745–1761 (2018).
29. M. Burke *et al.*, The changing risk and burden of wildfire in the United States. *Proc. Natl. Acad. Sci. U.S.A.* **118**, e2011048118 (2021).
30. K. O'Dell *et al.*, Estimated mortality and morbidity attributable to smoke plumes in the United States: Not just a Western US problem. *GeoHealth* **5**, e2021GH000457 (2021).
31. S. Heft-Neal *et al.*, Emergency department visits respond nonlinearly to wildfire smoke. *Proc. Natl. Acad. Sci. U.S.A.* **120**, e2302409120 (2023).
32. A. Swanson *et al.*, Daily 1 km terrain resolving maps of surface fine particulate matter for the Western United States 2003–2021. *Sci. Data* **9**, 1–13 (2022).
33. National Oceanic and Atmospheric Administration, Hazard mapping system fire and smoke product. https://www.ospo.noaa.gov/Products/land/hms.html#about. Accessed 20 January 2020.
34. National Oceanic and Atmospheric Administration, NOAA Geostationary Operational Environmental Satellites (GOES) 16, 17 & 18. https://registry.opendata.aws/noaa-goes. Accessed 2 August 2022.
35. NASA Earth Observing System Data and Information System (EOSDIS), Moderate resolution imaging spectroradiometer (MODIS). https://worldview.earthdata.nasa.gov. Accessed 5 May 2023.
36. C. F. Gould *et al.*, Health effects of wildfire smoke exposure. *Ann. Rev. Med.* **75** (2023).
37. National Fire and Aviation Management (FAMWEB) and National Interagency Fire Center (NIFC), as reported by Headwaters Economics, Wildfires destroy thousands of structures each year (Headwaters Economics, 2022). https://headwaterseconomics.org/natural-hazards/structures-destroyed-by-wildfire. Accessed 18 October 2022.
38. P. Baylis, J. Boomhower, The economic incidence of wildfire suppression in the United States. *Am. Econ. J. Appl. Econ.* **15**, 442–473 (2023).
39. M. Jerrett, A. S. Jina, M. E. Marlier, Up in smoke: California's greenhouse gas reductions could be wiped out by 2020 wildfires. *Environ. Pollution* **310**, 119888 (2022).
40. T. Y. Wilmot, A. G. Hallar, J. C. Lin, D. V. Mallia, Expanding number of Western US urban centers face declining summertime air quality due to enhanced wildland fire activity. *Environ. Res. Lett.* **16**, 054036 (2021).
41. T. Y. Wilmot, D. V. Mallia, A. Gannet Hallar, J. C. Lin, Wildfire activity is driving summertime air quality degradation across the Western US: A model-based attribution to smoke source regions. *Environ. Res. Lett.* **17**, 114014 (2022).

42. H. Shi *et al.*, Modeling study of the air quality impact of record-breaking Southern California wildfires in December 2017. *J. Geophys. Res. Atmos.* **124**, 6554–6570 (2019).
43. U. Sofowote, F. Dempsey, Impacts of forest fires on ambient near–real–time $PM_{2.5}$ in Ontario, Canada: Meteorological analyses and source apportionment of the July 2011–2013 episodes. *Atmos. Pollution Res.* **6**, 1–10 (2015).
44. S. Viswanathan, L. Eria, N. Diunugala, J. Johnson, C. McClean, An analysis of effects of San Diego wildfire on ambient air quality. *J. Air Waste Manage. Assoc.* **56**, 56–67 (2006).
45. R. Munoz-Alpizar *et al.*, Multi-year (2013–2016) $PM_{2.5}$ wildfire pollution exposure over North America as determined from operational air quality forecasts. *Atmosphere* **8**, 179 (2017).
46. D. A. Jaffe *et al.*, Wildfire and prescribed burning impacts on air quality in the United States. *J. Air Waste Manage. Assoc.* **70**, 583–615 (2020).
47. E. E. McDuffie *et al.*, Source sector and fuel contributions to ambient $PM_{2.5}$ and attributable mortality across multiple spatial scales. *Nat. Commun.* **12**, 1–12 (2021).
48. S. N. Koplitz, C. G. Nolte, G. A. Pouliot, J. M. Vukovich, J. Beidler, Influence of uncertainties in burned area estimates on modeled wildland fire $PM_{2.5}$ and ozone pollution in the contiguous US. *Atmos. Environ.* **191**, 328–339 (2018).
49. I. N. Sokolik, A. J. Soja, P. J. DeMott, D. Winker, Progress and challenges in quantifying wildfire smoke emissions, their properties, transport, and atmospheric impacts. *J. Geophys. Res. Atmos.* **124**, 13005–13025 (2019).
50. M. V. Martin, C. L. Heald, B. Ford, A. J. Prenni, C. Wiedinmyer, A decadal satellite analysis of the origins and impacts of smoke in Colorado. *Atmos. Chem. Phys.* **13**, 7429–7439 (2013).
51. C. D. McClure, D. A. Jaffe, US particulate matter air quality improves except in wildfire-prone areas. *Proc. Natl. Acad. Sci. U.S.A.* **115**, 7901–7906 (2018).
52. Y. Ma *et al.*, Wildfire smoke $PM_{2.5}$ and mortality in the contiguous United States. medRxiv [Preprint] (2023). https://doi.org/10.1101/2023.01.31.23285059. Accessed 2 April 2023.
53. C. E. Reid *et al.*, Effect modification of the association between fine particulate air pollution during a wildfire event and respiratory health by area-level measures of socio-economic status, race/ethnicity, and smoking prevalence. *Environ. Res. Health* **1**, 025005 (2023).
54. G. Rein, X. Huang, Smouldering wildfires in peatlands, forests and the Arctic: Challenges and perspectives. *Curr. Opin. Environ. Sci. Health* **24**, 100296 (2021).
55. P. H. Gude, K. Jones, R. Rasker, M. C. Greenwood, Evidence for the effect of homes on wildfire suppression costs. *Int. J. Wildland Fire* **22**, 537–548 (2013).
56. M. V. Martin, R. A. Kahn, M. G. Tosca, A global analysis of wildfire smoke injection heights derived from space-based multi-angle imaging. *Remote Sensing* **10**, 1609 (2018).
57. A. Lyapustin, Y. Wang, S. Korkin, R. Kahn, D. Winker, Maiac thermal technique for smoke injection height from modis. *IEEE Geosci. Remote Sensing Lett.* **17**, 730–734 (2019).
58. T. Y. Wilmot, D. V. Mallia, A. Hallar, J. C. Lin, Wildfire plumes in the Western US are reaching greater heights and injecting more aerosols aloft as wildfire activity intensifies. *Sci. Rep.* **12**, 1–14 (2022).
59. R. E. Wolf, S. A. Morman, G. S. Plumlee, P. L. Hageman, M. Adams, Release of hexavalent chromium by ash and soils in wildfire-impacted areas (Tech. Rep. 1345, Open-File Report, U.S. Geological Survey, 2008). Accessed 1 March 2023.
60. K. Boaggio *et al.*, Beyond particulate matter mass: Heightened levels of lead and other pollutants associated with destructive fire events in California. *Environ. Sci. Technol.* **56**, 14272–14283 (2022).
61. J. P. S. Wong *et al.*, Effects of atmospheric processing on the oxidative potential of biomass burning organic aerosols. *Environ. Sci. Technol.* **53**, 6747–6756 (2019).
62. John T. Abatzoglou *et al.*, Projected increases in Western US forest fire despite growing fuel constraints. *Commun. Earth Environ.* **2**, 1–8 (2021).
63. Y. Xie *et al.*, Tripling of Western US particulate pollution from wildfires in a warming climate. *Proc. Natl. Acad. Sci. U.S.A.* **119**, e2111372119 (2022).
64. G. Chen *et al.*, Mortality risk attributable to wildfire-related $PM_{2.5}$ pollution: A global time series study in 749 locations. *Lancet Planet. Health* **5**, e579–e587 (2021).
65. S. M. Holm, M. D. Miller, J. R. Balmes, Health effects of wildfire smoke in children and public health tools: A narrative review. *J. Expo. Sci. Environ. Epidemiol.* **31**, 1–20 (2021).
66. M. Borgschulte, D. Molitor, E. Zou, Air pollution and the labor market: Evidence from wildfire smoke. *Rev. Econ. Stat.* 1–46 (2022).
67. A. F. Stein *et al.*, NOAA's hysplit atmospheric transport and dispersion modeling system. *Bull. Am. Meteorol. Soc.* **96**, 2059–2077 (2015).
68. G. D. Rolph *et al.*, Description and verification of the NOAA smoke forecasting system: The 2007 fire season. *Weather Forecast.* **24**, 361–378 (2009).
69. T. Artés *et al.*, A global wildfire dataset for the analysis of fire regimes and fire behaviour. *Sci. Data* **6**, 1–11 (2019).
70. A. Benali *et al.*, Determining fire dates and locating ignition points with satellite data. *Remote Sensing* **8**, 326 (2016).
71. I. Csiszar *et al.*, Active fires from the Suomi NPP visible infrared imaging radiometer suite: Product status and first evaluation results. *J. Geophys. Res. Atmos.* **119**, 803–816 (2014).
72. WorldPop and Center for International Earth Science Information Network, Columbia University, Global 1 km population total adjusted to match the corresponding UNPD estimate (2020). University of Southampton. https://dx.doi.org/10.5258/SOTON/WP00671. Accessed 2 June 2022.
73. California Department of Health Care Access and Information, Nonpublic emergency department data: Individual emergency department encounters. https://hcai.ca.gov/data-and-reports/healthcare-utilization/emergency-department/. Accessed 23 July 2019.
74. J. Wen *et al.*, Quantifying fire-specific smoke exposure and health impacts. Replication materials. https://github.com/jeffwen/smoke_linking_public. Deposited 8 November 2023.